Paper to be presented at the AMS Sixth Conference on Climate Variations, January 1994, Nashville, Tennessee.



# IMPACT OF CLOUD MICROPHYSICS ON CLOUD-RADIATION INTERACTIONS IN THE CSU GENERAL CIRCULATION MODEL

Laura D. Fowler and David A. Randall

*Department of Atmospheric Science*
*Colorado State University*
*Fort Collins, Colorado*

## 1. INTRODUCTION

Our ability to study and quantify the impact of cloud-radiation interactions in studying global scale climate variations strongly relies upon the ability of general circulation models (GCMs) to simulate the coupling between the spatial and temporal variations of the model-generated cloudiness and atmospheric moisture budget components. In particular, the ability of GCMs to reproduce the geographical distribution of the sources and sinks of the planetary radiation balance depends upon their representation of the formation and dissipation of cloudiness in conjunction with cloud microphysics processes, and the fractional amount and optical characteristics of cloudiness in conjunction with the mass of condensate stored in the atmosphere.

A cloud microphysics package which encompasses five prognostic variables for the mass of water vapor, cloud water, cloud ice, rain, and snow has been implemented in the Colorado State University General Circulation Model (CSU GCM) to simulate large-scale condensation processes. Convection interacts with the large-scale environment through the detrainment of cloud water and cloud ice at the top of cumulus towers. The cloud infrared emissivity and cloud optical depth of the model-generated cloudiness are interactive and depend upon the mass of cloud water and cloud ice suspended in the atmosphere.

The global atmospheric moisture budget and planetary radiation budget of the CSU GCM obtained from a perpetual January simulation are discussed. Geographical distributions of the atmospheric moisture species are presented. Global maps of the top-of-atmosphere outgoing longwave radiation and planetary albedo are compared against Earth Radiation Budget Experiment (ERBE) satellite data.

## 2. CLOUD MICROPHYSICS MODEL

The model structure is largely based upon the bulk cloud microphysics equations of the mesoscale cloud models described in Lin *et al.* (1983), and Rutledge and Hobbs (1983; 1984). Five prognostic variables for the mass of water vapor, cloud water, cloud ice, rain, and snow are considered. Cloud water and cloud ice are predicted to form through large-scale condensation and deposition processes. An important additional source of cloud water and ice is by detrainment at the top of cumulus towers. Like these previous studies, we assume that the fallspeed of cloud water and ice particles is negligible. Rain and snow are assumed to have non-negligible fall velocities. A detailed description of the bulk cloud microphysics equations is given in Fowler and Randall (1993a).

Water vapor is a source of cloud water and cloud ice. Cloud water is predicted to form by condensation of vapor when the temperature (T) is equal or greater than $T_o = 0°C$ and the air is supersaturated with respect to water. Cloud ice is predicted to form by deposition of vapor if $T<T_o$ and the air is supersaturated with respect to ice. Supercooled cloud water and cloud ice may coexist in the temperature range $T_{oo} \le T < T_o$. $T_{oo}$ is equal to -40°C for consistency with the cumulus convection scheme, and the saturation vapor pressure at temperatures between $T_{oo}$ and $T_o$ is obtained by linear interpolation between the saturation vapor pressures with respect to water and ice. Water vapor may also be a source of rain and snow by condensation and deposition, respectively.

Cloud water is a source for water vapor by evaporation of cloud droplets in a subsaturated layer or a source of rain if the air remains supersaturated. The conversion of cloud water to rain occurs through two different mechanisms: (1) autoconversion of cloud water to form rain; and (2) collection of cloud water by rain. Supercooled cloud water is also a source of ice by instantaneous freezing ($T < T_{oo}$), or through the Bergeron process ($T_{oo} \le T < T_o$), or a source of snow by riming.

Similar to cloud water, cloud ice is a source for water vapor by sublimation when the air is subsaturated with respect to ice. Otherwise, cloud ice is a source of

snow through two different mechanisms: (1) autoconversion of cloud ice to form snow; and (2) collection of cloud ice by snow. Instantaneous melting of cloud ice to form cloud water occurs if $T \geq T_o$.

Rain is a source for water vapor by evaporation. Rain may also be a source of snow by instantaneous freezing if $T < T_o$.

Similar to rain, snow is a source for water vapor by sublimation. Also, snow may be a source of rain by melting ($T \geq T_o$).

Fowler and Randall (1993a) extensively describe the implicit scheme used to compute the change in water vapor, cloud water, cloud ice, rain, and snow due to the combined cloud microphysics processes, as well as the falling of rain and snow through the model atmosphere.

## 3. CLOUD-RADIATION INTERACTIONS

The parameterization of the radiation transfer at infrared and solar wave lengths is described by Harshvardhan *et al.* (1987). Modifications to the original scheme are listed in Harshvardhan *et al.* (1989). At the present time, the cloud microphysics and radiation transfer schemes do not allow fractional cloudiness. No clouds are allowed to form in the two highest model layers located between the tropopause level (fixed at 100 mb) and the model upper boundary located at 51.3 mb. The computation of the fractional amount of planetary boundary layer (PBL) clouds follows the formulation of Harshvardhan *et al.* (1989), and Randall *et al.* (1989). The fractional area of clouds predicted to form above the PBL top is set equal to 1 if the cloud water or ice paths is greater than 1 g $m^{-2}$ in the model layer.

The formulation of the cloud radiative properties as a function of the cloud water and ice paths simply follows the formulation of Stephens (1978). The cloud optical depth ($\tau$) and cloud infrared emissivity ($\varepsilon$) are computed following the relations:

$$\tau = \frac{3W}{2r_e} \quad \text{and} \quad \varepsilon = 1 - \exp(-\kappa W) \qquad (1)$$

where W is the cloud water or ice path (in g $m^{-2}$). The effective radius ($r_e$; in $\mu$m) is set equal to 10 $\mu$m and 30 $\mu$m for cloud water and cloud ice, respectively. The absorption coefficient ($\kappa$; in $m^2$ $g^{-1}$) is set equal to 0.13 and 0.08 for cloud water and cloud ice, respectively. The single scattering albedo ($\omega_0$) and the asymmetry factor (g) are assumed to be the same for cloud water and cloud ice. In this simulation, $\omega_0$ is equal to 0.99 and g is set to 0.85.

## 4. MODEL RESULTS

The model was run for 60 days under perpetual January conditions, with initial amounts of cloud water, cloud ice, rain, and snow set to zero. The model physics is computed every hour while the model dynamics is run using a time-step of six minutes. The cloud microphysics package is embedded in the dynamics package and is run every two minutes to properly describe the falling of rain and snow through the model atmosphere. Results correspond to 30-day means obtained from the last 30 days of the model simulation.

Figure 1 shows the geographical distributions of the vertically-integrated cloud water (CW), cloud ice (CI), rain (RW), and snow (RI) amounts obtained with the cloud microphysics scheme. Maxima of CW, CI, and then RW and RI, are located over the major storm track regions over the oceans in conjunction with midlatitude cyclogenetic activity, and over the chief tropical convective activity regions in conjunction with maximum detrainment of cloud water and cloud ice from cumulus detrainment. In January, these maxima may be observed above the North Pacific and North Atlantic Oceans, and above South America, Southern Africa in the middle latitudes, and the winter monsoon region over Malaysia and Northern Australia at equatorial latitudes. In contrast to Fig.1, the latitude versus height cross sections of the zonally-averaged fields (refer to Fowler and Randall, 1993a) shows that CI is actually the largest above the deep convective regions, below the tropopause level, and gradually decreases poleward. Areas of maximum amounts of CI and RI appear to be more widely spread than those of CW and RW, respectively. The relative magnitude of CW versus CI is shown to be strongly dependent upon the Bergeron process. In Fig. 1, supercooled cloud water is accounted for as CW. Also the relative magnitude of CW versus RW, and more importantly CI versus RI, is strongly dependent upon the threshold values used for autoconversion of cloud water to rain, and cloud ice to snow. These threshold values were chosen so that reasonable cloud optical properties may be obtained. Sensitivity tests have been done to estimate the impact of the autoconversion processes upon the magnitude of CW, RW, CI, and RI, and then the planetary radiation balance components (Fowler and Randall, 1993b).

Figure 2 shows the geographical distributions of the top-of-atmosphere outgoing longwave radiation (IR) and planetary albedo ($\alpha$) obtained with the CSU GCM for January perpetual conditions versus ERBE observations. The satellite data is a January ensemble average between 1985 and 1988, interpolated over the GCM grid. The GCM reproduces very successfully the global distribution and intensity of IR, especially above

## DISCLAIMER

the deep tropical convective regions. On a global average, the model-simulated IR is equal to 227 W $m^{-2}$ versus 232 W $m^{-2}$ from ERBE. Areas of low IR above South America, Southern Africa, and the winter monsoon region coincide very well with satellite observations. However, the IR is too cold by as much as 15 W $m^{-2}$ at high latitudes, especially in the winter hemisphere. The GCM underestimates the extent of the belt of high IR across Africa and India. Also it has to be pointed out that the inability of the GCM to realistically simulate the planetary boundary layer clouds along the western coasts of the continents causes the oceanic belts of high IR to be positioned too close to the shore. The model-generated $\alpha$ does not agree as well as the IR when compared against satellite observations, and is generally too low. The GCM systematically underestimates the magnitude of $\alpha$ over both cloudy and cloud-free regions over land. In particular, $\alpha$ is about 5% smaller than actually observed over the deep tropical convective activity regions. The increase in $\alpha$ at high latitudes is very poorly simulated, especially in the winter hemisphere.

## 5. CONCLUSIONS

Results of a 60-day perpetual January simulation obtained with the CSU General Circulation which includes a new cloud microphysics scheme and interactive cloud optical properties are very encouraging.The model produces geographical distributions of the cloud water, cloud ice, rain, and snow that appear to be very reasonable. Validation of the cloud water against SSMI satellite observations is being undertaken. Quantitatively, it remains quite impossible to validate the magnitude of the model-generated cloud ice amount, except at very limited regional scales or in terms of the resulting outgoing longwave radiation and planetary albedo. The sensitivity of the planetary radiation balance components to the cloud optical properties is being analyzed with the aim to improve the distribution of the outgoing longwave radiation at polar latitudes, and the planetary albedo over cloudy areas. Rain and snow amounts may be validated in terms of the surface precipitation rates that they produce.

In view of our results, several important questions may be addressed:

1. As shown in Fig. 1, the model produces large amounts of snow falling slowly to the model surface. It is very likely that this snow would have a strong radiative impact. What would be the impact of including the radiative effect of snow upon the planetary radiation balance, especially at short wave lengths?

2. The fractional cloud cover is set to 1, except for the PBL clouds. How would the atmospheric moisture budget components, and then the cloud optical properties, be modified if the model allowed for some kind of fractional cloud amount?

## REFERENCES


Fowler, L.D., and D.A. Randall, 1993a: Liquid and ice cloud microphysics in the CSU General Circulation Model. Part I: Model description and results of a baseline simulation (In preparation.)

Fowler, L.D., and D.A. Randall, 1993b: Liquid and ice cloud microphysics in the CSU General Circulation Model. Part II: Sensitivity experiments (In preparation.)

Harshvardhan, R. Davies, D.A. Randall, and T.G. Corsetti, 1987: A fast radiation parameterization for atmospheric circulation models. *J. Geophys. Res.*, **92 D1,** 1009-1016.

Harshvardhan, D.A. Randall, T.G. Corsetti, and D.A. Dazlich, 1989: Earth Radiation Budget and cloudiness simulations with a general circulation model. *J. Atmos Sci.*, **46,** 1922-1942.

Lin, Y.-L., R.D. Farley, and H.D. Orville, 1983: Bulk parameterization of the snow field in a cloud model. *J. Atmos. Sci.*, **22,** 1065-1092.

Randall, D.A., Harshvardhan, D.A. Dazlich, and T.G. Corsetti, 1989: Interactions among radiation, convection, and large-scale dynamics in a general circulation model. *J. Atmos. Sci.*, **46,** 1943-1970.

Rutledge, S.A., and P.V. Hobbs, 1983: The mesoscale and microscale structure and organization of cloud bands and precipitation in midlatitude cyclones. VIII: A model for the "Seeder Feeder" process in warm-frontal bands. *J. Atmos. Sci.*, **40,** 1185-1206.

Rutledge, S.A., and P.V. Hobbs, 1984: The mesoscale and microscale structure of clouds and precipitation in midlatitude cyclones. XII: A diagnostic modeling study of precipitation development in narrow cold-frontal rainbands. *J. Atmos. Sci.*, **41,** 2949-2972.

Stephens, G.L., 1978: Radiation profiles in extended water clouds. Part II: Parameterization schemes. *J. Atmos. Sci.*, **46,** 1419-1427.


## ACKNOWLEDGMENTS


This research was sponsored by the National Science Foundation under the grant ATM-8907414 and the Department of Energy under the grant DE FG02-91ER61218.

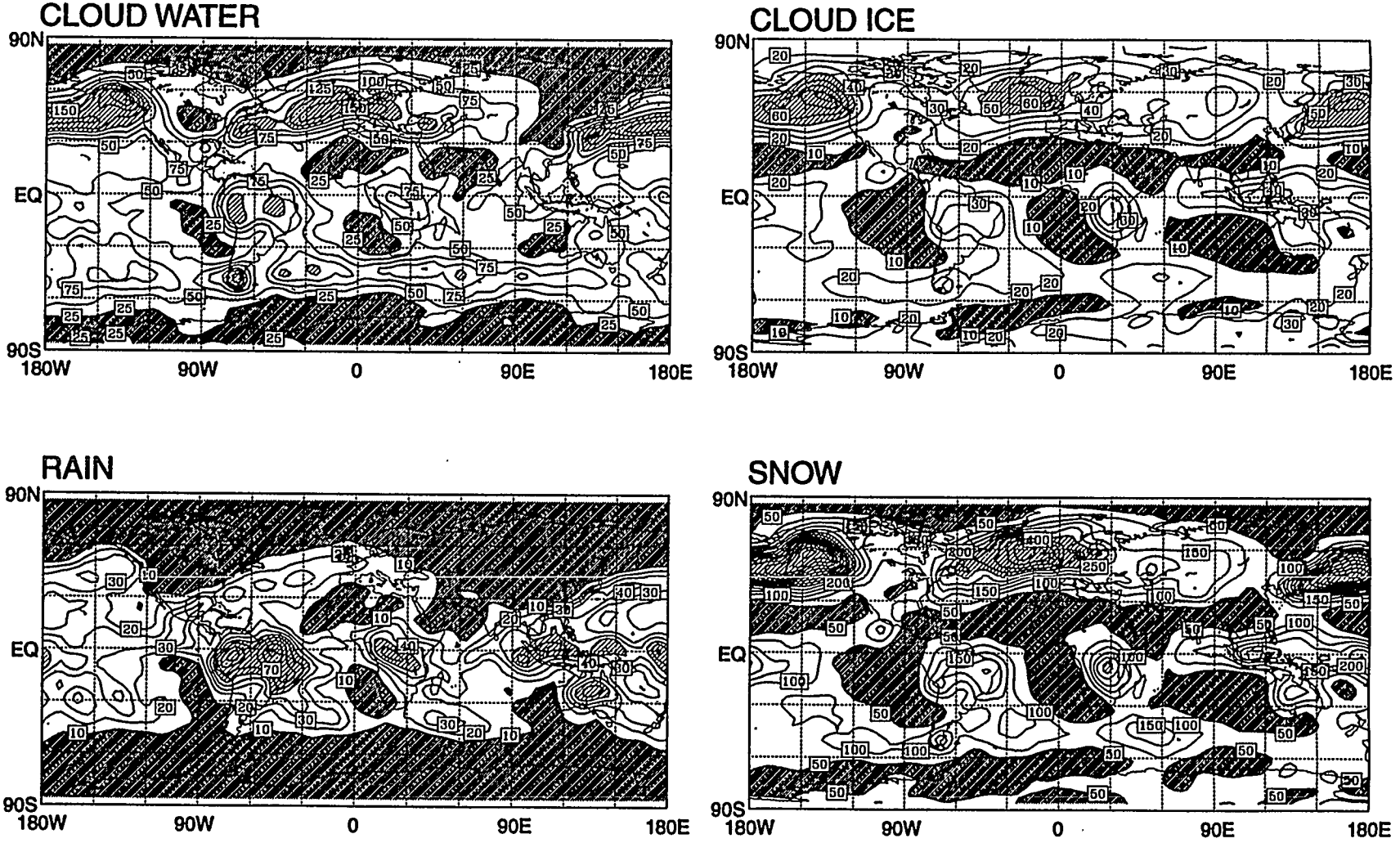


Figure 1: Geographical distributions of the vertically-integrated atmospheric moisture variables obtained with the CSU GCM for January conditions (g $m^{-2}$). The contour intervals are 25 g $m^{-2}$ for the cloud water, 10 g $m^{-2}$ for the cloud ice, 10 g $m^{-2}$ for the rain, and 50 g $m^{-2}$ for the snow, respectively. Dark shading corresponds to values less than 25, 10, 10, and 50 g $m^{-2}$ for the cloud water, cloud ice, rain, and snow. Light shading corresponds to values greater than 125, 50, 50, and 500 g $m^{-2}$ for the cloud water, cloud ice, rain, and snow, respectively.

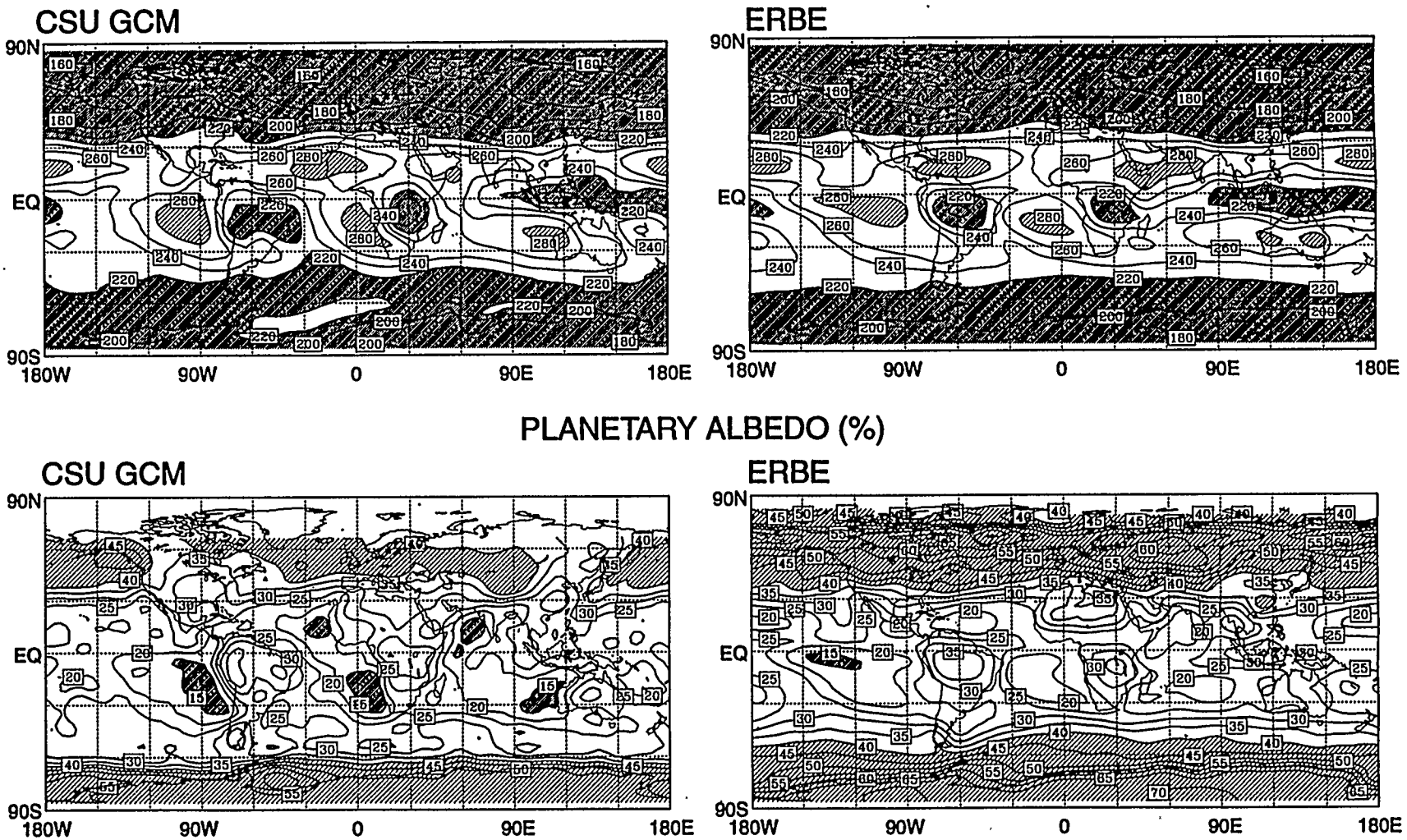


Figure 2: Geographical distributions of the planetary radiation balance components obtained with the CSU GCM for January conditions (left-hand side panel) versus ERBE satellite data (right-hand side panel). For the outgoing longwave radiation, dark (light) shading corresponds to values less (greater) than 220 W $m^{-2}$ (280 W $m^{-2}$). For the planetary albedo, dark (light) shading corresponds to values less (greater) than 15% (40%).